

Article

Enhanced Soft Magnetic Properties of Iron-Based Powder Cores with Co-Existence of Fe_3O_4 – $\text{MnZnFe}_2\text{O}_4$ Nanoparticles

Yuye Xie ^{1,2}, Pengfei Yan ³ and Biao Yan ^{1,2,*}

¹ School of Materials Science and Engineering, Tongji University, Shanghai 201804, China; 1251713@tongji.edu.cn

² Shanghai Key Laboratory for R&D and Application of Metallic Functional Materials, Shanghai 201804, China

³ School of Physics Science and Engineering, Tongji University, Shanghai 20082, China; 18310048@tongji.edu.cn

* Correspondence: 84016@tongji.edu.cn; Tel.: +86-133-118-90331

Received: 6 August 2018; Accepted: 4 September 2018; Published: 6 September 2018



Abstract: An iron-based soft magnetic composite with Fe_3O_4 - $\text{MnZnFe}_2\text{O}_4$ insulation coating has been prepared by powder metallurgy method. This work investigated the microstructure and magnetic properties of Fe/ Fe_3O_4 - $\text{MnZnFe}_2\text{O}_4$ powder cores. Scanning electron microscopy (SEM) coupled with an energy dispersive spectrometry (EDS) analysis indicated that the Fe_3O_4 and $\text{MnZnFe}_2\text{O}_4$ nanoparticles were uniformly coated on the surface of Fe powders. The co-existence of Fe_3O_4 and $\text{MnZnFe}_2\text{O}_4$ contributes to the preferable distribution of nano-sized insulation powders and excellent soft magnetic properties of soft magnetic composite (SMC) with high saturation magnetization M_s (215 A·m²/kg), low core loss (178.7 W/kg measured at 100 kHz, 50 mT), and high effective amplitude permeability of 114 (measured at 100 kHz). Overall, this work has great potential for realizing low core loss and outstanding soft magnetic properties of Fe-based powder cores.

Keywords: soft magnetic composite; ferrite; powder metallurgy; low core loss

1. Introduction

Soft magnetic composites (SMCs), as reported by H. Shokrollahi in 2007 [1], are considered as advanced electrical inductance materials. SMCs can be described as ferromagnetic powders that are surrounded by a thin but electrically insulating layer and pressed into cores by easy powder metallurgy methods. Compared with the conventional laminated steel cores, SMCs offer enormous advantages, such as three-dimensional isotropic magnetic properties, low eddy-current core loss at high frequency, and high adaptability to complex machine design. Hence, it has replaced the laminated steel cores in most fields of electric motors, transformer cores, power switching inductors, online noise filters, and chokes [2–5].

With the increasing demands of electromagnetic devices at high frequency, improving the magnetic performance of SMCs is of crucial importance [6]. The challenge in current SMCs is obtaining low eddy-current core loss at high frequency, high magnetic permeability, and high thermal stability of the materials [7,8]. Eddy-current loss can be minimized in several ways. The latest technology is to increase the electrical resistivity of the insulating coatings [1]. Besides, to improve the magnetic permeability, the amount of insulation coatings on the surface should be minimized, and the ferromagnetic powder content maximized [9]. Thus, many studies have been carried out to develop suitable insulating materials and proper manufacturing methods in order to improve the soft magnetic properties of SMCs. Generally, the insulating materials are divided into organic and inorganic materials. Organic materials such as epoxy resin [10], parylene [11], and phenolic resin [12]

exhibit a satisfactory performance in increasing the resistivity of iron powders, but their application under high temperatures is limited due to the nature of high polymer materials. Inorganic coating can therefore be a better choice, since, if the proper amount of coating material is applied, they have high thermal stability and improved soft magnetic properties. Inorganic coating materials are divided into two different types. Ceramic materials which are dia- or anti-ferromagnetic constitute one type. These materials—such as Al_2O_3 [13], SiO_2 [14], and ZrO_2 [15]—which can significantly decrease the core loss at a high frequency, also decrease magnetic permeability by reducing the proportion of magnetic materials. Materials that exhibit ferro- or ferrimagnetism, which can ultimately affect the core loss and improve the magnetic permeability compared with the ceramic coating materials, constitute the other type. It was found that the use of nanoparticles of Fe_3O_4 resulted in an improvement in soft magnetization [16]. However, Fe_3O_4 is a semiconductor with a resistivity of $10^{-2} \Omega\cdot\text{cm}$, so the eddy-current core loss will increase quickly as the frequency increases [17]. $\text{MnZnFe}_2\text{O}_4$ ferrite has been used in many applications such as radio frequency circuits and transformer cores due to its high electrical resistivity.

In this study, a novel SMC which was covered by Fe_3O_4 and $\text{MnZnFe}_2\text{O}_4$ nanoparticles was prepared. The Fe_3O_4 nanoparticles were dispersed uniformly in the as-prepared $\text{MnZnFe}_2\text{O}_4$ gel to form a uniform coating on the iron powders. Moreover, the simultaneous incorporation of Fe_3O_4 and $\text{MnZnFe}_2\text{O}_4$ resulted in the high magnetic saturation, high permeability, and reduced eddy-current core loss.

2. Materials and Methods

2.1. Materials

Pure atomized iron powder with an average particle size of $75 \mu\text{m}$ was supplied by An Gang Industries Co., Ltd. (Anshan, China), Nano- Fe_3O_4 powders (purity > 99.99%, 20 nm) were purchased from Aladdin biochemical Polytron Technologies Company (Shanghai, China) and used without further treatment. $\text{MnZnFe}_2\text{O}_4$ manufactured by a novel sol-gel auto-combustion method was used as the insulation material. Analytically pure chemicals manganese nitrate solution (50 wt. % in H_2O , Aladdin), zinc nitrate hexahydrate (99%, Aladdin), and iron nitrate nonahydrate (99%, Aladdin) were dissolved in deionized water and citric acid (99.8%, Aladdin) to prepare the soft magnetic MnZn ferrites.

2.2. Preparation of As-Prepared MnZn Ferrite Sol

Manganese nitrate solution, zinc nitrate hexahydrate, and iron nitrate nonahydrate were dissolved in deionized water and citric acid. Then the mixture was heated to 75°C in an oil bath and mixed evenly in a three-necked round bottom flask under magnetic stirring. Ammonia was subsequently added as the catalyst to adjust the PH value to about 5 and shorten the gel time. The resulting mixture was maintained under magnetic stirring at 75°C for 4 h.

2.3. Composite Production

The Nano- Fe_3O_4 powders were mixed with the as-prepared MnZn ferrite sol by ultrasonic treatment to prevent the agglomeration of nanoparticles. The powder mixture was dried at 100°C for 1 h to get the gel. Then the gel was coated on the iron powders by mechanic stirring and auto-combustion. The effect of the content of MnZn ferrites (0.5–3 wt. %) and Nano- Fe_3O_4 powders (0.5–3 wt. %) is discussed in this paper. The coated iron powders were compacted at 800 MPa in a die with 0.5 wt. % zinc stearate as the lubricant. This process resulted in a ring shapes composite with an outer diameter of 20 mm, an inner diameter of 12 mm, and a thickness of 3 mm. The schematic formation process is shown in Figure 1.

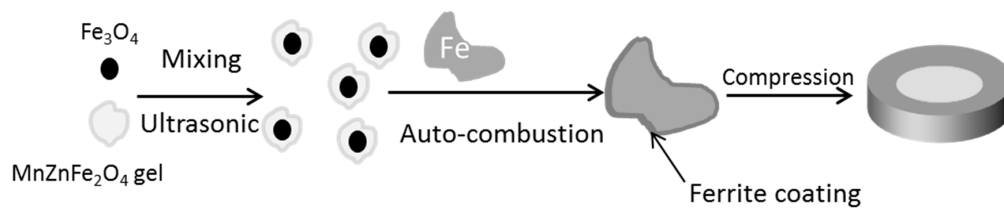


Figure 1. Procedure for Fe_3O_4 and MnZn ferrite insulation coated iron powder.

2.4. Material Characterization

The crystal structure analysis and morphology of the resulting product were carried out by X-ray powder diffraction (XRD) (DX-2007, Dandong Fang Yuan Co., Ltd, Dandong, China) with $\text{Cu } K_\alpha$ diffraction at 30 kV and 30 mA at room temperature, and scanning electron microscopy (SEM, Nova NanoSEM 450, FEI, Hillsboro, OR, USA) equipped with an energy dispersive spectroscopy (EDS) (Ultra, EDAX, Mahwah, NJ, USA). The chemical state of coating was identified by X-ray photoelectron spectroscopy (XPS, 250XI, Thermo Fisher, Waltham, MA, USA). The densities of powder cores were determined by Archimedes principle with ethanol as the immersion fluid in the densimeter (ZMD-2, Shanghai Fangrui Instrument Co., Ltd, Shanghai, China). The electrical resistivities of the powder cores were measured by the four-point probe method. The magnetic properties of the samples, such as the saturation magnetization (M_s) and remnant magnetization (M_r), were measured by vibrating sample magnetometer (VSM, Lakeshore 7407, Columbus, OH, USA) at room temperature. The amplitude permeability and core loss of the samples were investigated by a soft magnetic AC measuring instrument (MATS-2010SA/500k, Linkioin, Loudi, China) at a magnetic excitation level of 50 mT and the frequency range from 5 kHz to 100 kHz. The D-C magnetic property was recorded using a soft magnetic DC measuring instrument (MATS-2010SD, Linkioin, Loudi, China) under the maximum applied magnetic field of 45,000 A/m.

3. Results and Discussion

3.1. Characterization of the Soft Magnetic Composites

The SEM images of iron and iron powders after the coating process are shown in Figure 2. Obviously, the surface of the coated composite (Figure 2b) shows rough morphologies with many fine particles compared with the smooth surface morphologies of the typical water-atomized powders (Figure 2a). It can be seen that the nanoparticles of Fe_3O_4 and $\text{MnZnFe}_2\text{O}_4$ are uniform and regular in size and shape (inset in Figure 2b). The coating of the iron powder surface by ferrites is indirectly shown in Figure 3, and the existence of iron, manganese, zinc, and oxygen clearly indicates the presence of Fe_3O_4 - $\text{MnZnFe}_2\text{O}_4$ ferrite coating on the surface of the water-atomized iron powders.

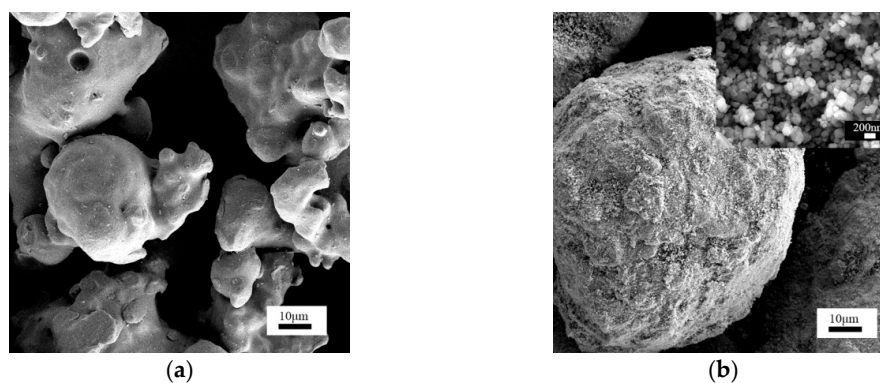


Figure 2. (a) SEM image of iron powders; (b) SEM image of coated iron powders.

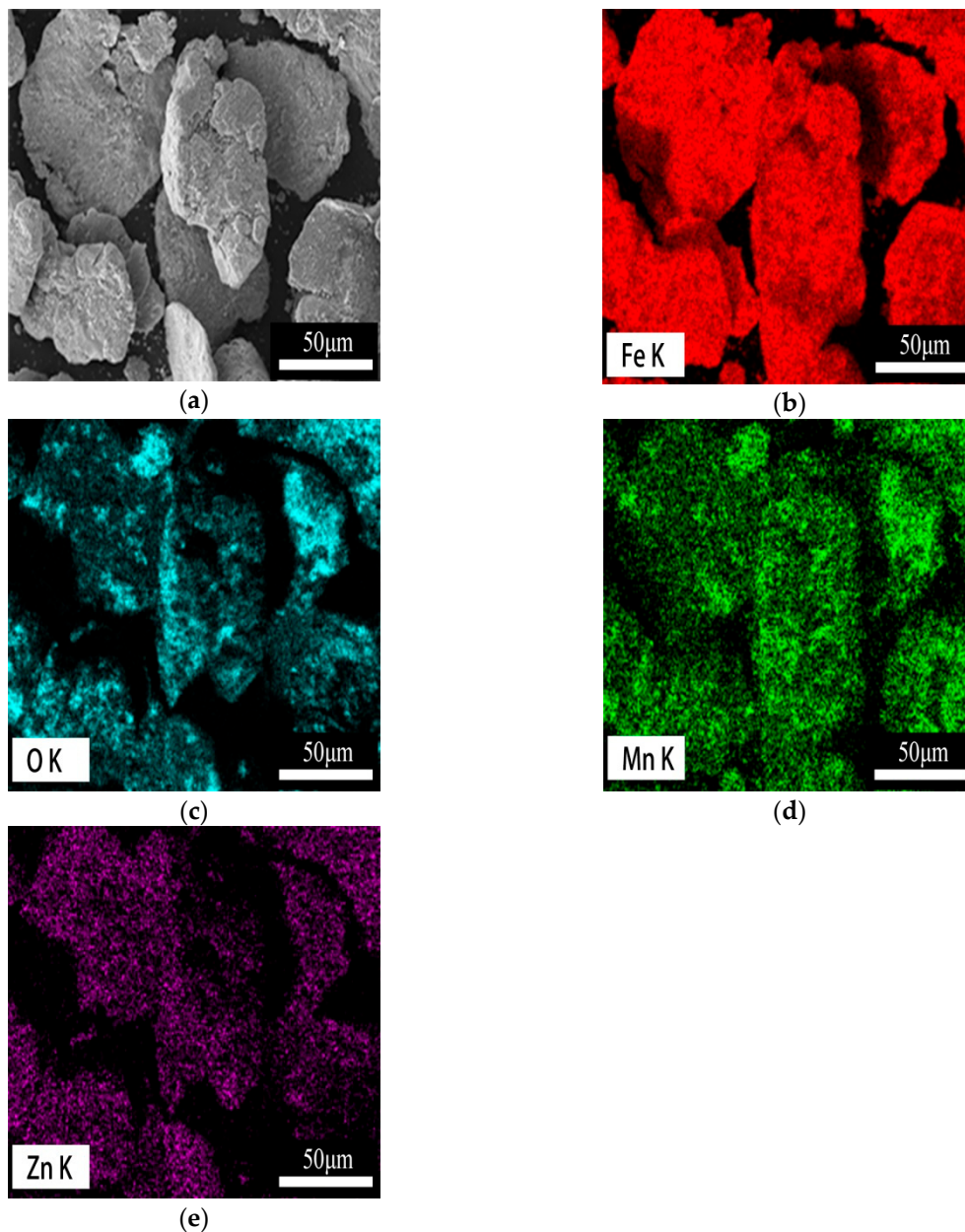


Figure 3. Cross-section SEM image of $\text{Fe}_3\text{O}_4\text{-MnZnFe}_2\text{O}_4$ coated iron powders (a) and EDS mapping of Fe (b), O (c), Mn (d), Zn (e).

Furthermore, as shown in Figure 4, the XRD pattern revealed the existence of the $\text{Fe}_3\text{O}_4\text{-MnZnFe}_2\text{O}_4$ ferrite phase on the surface of iron powders. According to the JCPDS card, Bragg peaks of low intensity centered at 2θ of 30° , 35° , 43° , 53° , 57° and 63° can be ascribed to the (220), (331), (400), (422), (511), and (440) planes of the $\text{Fe}_3\text{O}_4\text{-MnZnFe}_2\text{O}_4$ ferrite coating. It is clear that there are no other extra Bragg peaks in the composite powders, except those corresponding to the diffraction peaks of iron and $\text{Fe}_3\text{O}_4\text{-MnZnFe}_2\text{O}_4$ ferrite. This observation can also be confirmed by the previous EDS mapping analysis (Figure 3).

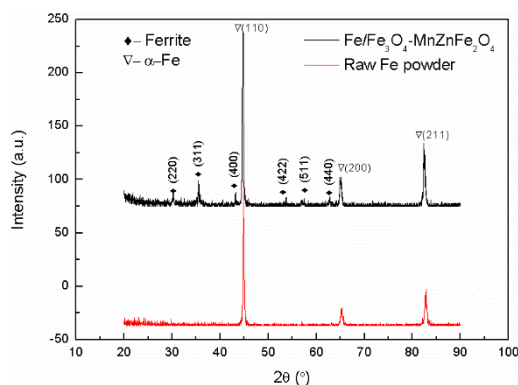


Figure 4. XRD pattern of raw iron powders and $\text{Fe}_3\text{O}_4\text{-MnZnFe}_2\text{O}_4$ coated iron powders.

As the Fe_3O_4 and $\text{MnZnFe}_2\text{O}_4$ shows similar XRD profiles but different valences of the Fe ion [18], XPS characterization was carried out to determine the chemical state of Fe ion. In the survey spectrum (Figure 5a), the elements, Mn, Zn, and Fe can be observed. Two main peaks of Fe $2p_{1/2}$ and Fe $2p_{3/2}$ which located at 710.9 eV and 724.3 eV were observed in the high-resolution XPS spectrum of Fe 2p in Figure 5b. In addition, a satellite peak, located at 718.5 eV, indicates the presence of Fe^{3+} [19]. The Fe^{3+} and Fe^{2+} ions were assumed to generate overlapping Fe 2p spectra. In order to identify the detailed chemical state of the Fe ion, the peaks were deconvoluted into two peaks. Fe_3O_4 is alternatively expressed as $\text{FeO}\cdot\text{Fe}_2\text{O}_3$, which is the chemical state of a mixture of Fe^{3+} and Fe^{2+} [19]. As shown in Figure 5b, the Fe 2p peaks fitted well with the Fe^{3+} and Fe^{2+} peaks, indicating that the oxidation layer consists of Fe_3O_4 .

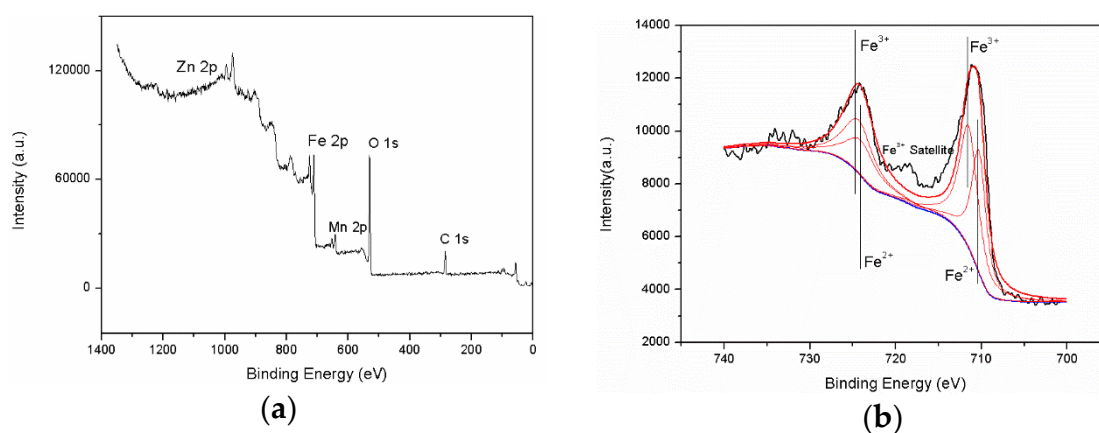


Figure 5. (a) XPS spectra of $\text{Fe}_3\text{O}_4\text{-MnZnFe}_2\text{O}_4$ coated iron powders, (b) fitted Fe 2p peaks.

To further indicate the uniformity of the insulation coating on the iron powders, an SEM image of the cross section of the composite was taken, as shown in Figure 6. It can be observed from Figure 6 that the insulation parts were uniformly distributed around the iron particles. The boundary of pure iron particles is almost 2 μm thick. This result further verified that the iron powders are uniformly covered by the nanoparticles of ferrites.

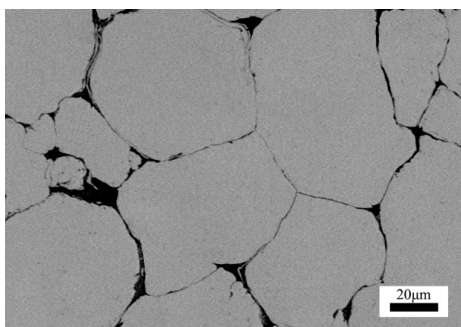


Figure 6. Cross section SEM image of Fe_3O_4 - $\text{MnZnFe}_2\text{O}_4$ coated iron-based composite.

3.2. Electrical and Magnetic Properties of the Composites

Magnetic hysteresis loops for Fe, $\text{Fe}/\text{Fe}_3\text{O}_4$ - $\text{MnZnFe}_2\text{O}_4$, Fe_3O_4 , and $\text{MnZnFe}_2\text{O}_4$ powders are shown in Figure 7. The loops revealed the typical magnetic behavior of SMCs, at an external field of $\sim 30,000$ Oe. The magnetic parameters such as M_s , M_r , and the ratio of remnant magnetization to saturation magnetization (M_r/M_s) are clearly presented in Table 1. It is found that the saturation magnetization of $\text{Fe}/\text{Fe}_3\text{O}_4$ - $\text{MnZnFe}_2\text{O}_4$ powders ($215.6 \text{ A}\cdot\text{m}^2/\text{kg}$) is slightly lower than that of Fe powder ($219.5 \text{ A}\cdot\text{m}^2/\text{kg}$) but higher than that of Fe_3O_4 powders ($84.1 \text{ A}\cdot\text{m}^2/\text{kg}$) and $\text{MnZnFe}_2\text{O}_4$ powders ($33.2 \text{ A}\cdot\text{m}^2/\text{kg}$). This result demonstrated that the ferrimagnetic insulation coating has a positive effect on the saturation magnetization of SMC. The M_s value of composite iron powders decreased as the percentage of magnetic Fe_3O_4 - $\text{MnZnFe}_2\text{O}_4$ phase increased. When the percentage of Fe_3O_4 - $\text{MnZnFe}_2\text{O}_4$ increased from 1 wt. % to 6 wt. %, the M_s decreased from $215 \text{ A}\cdot\text{m}^2/\text{kg}$ to $207 \text{ A}\cdot\text{m}^2/\text{kg}$. As shown in the Figure 7 and Table 1, the M_r value has nearly the same trend as M_s and a similar reason can be used to explain this phenomenon. It can also be seen from Table 1 that M_r/M_s shows no change with the increasing percentage of the ferrimagnetism insulation coating. This means that the value of M_r/M_s has nothing to do with the content of the Fe_3O_4 - $\text{MnZnFe}_2\text{O}_4$ phase.

The direct current performance and densities for the toroidal samples with different ferrite percentage at the maximum applied field of $45,000 \text{ A/m}$ are shown in Table 2. The coercivity increased as the content of Fe_3O_4 and $\text{MnZnFe}_2\text{O}_4$ increased from 1 wt. % to 6 wt. %. Moreover, the density decreased from 7.56 g/cm^3 to 6.92 g/cm^3 as the content of Fe_3O_4 and $\text{MnZnFe}_2\text{O}_4$ increased from 0 wt. % to 6 wt. %. It is easy to understand that, with the increasing of ferrite, the low density of Fe_3O_4 and $\text{MnZnFe}_2\text{O}_4$ leads to a decrease in the overall density of the composite. The maximum relative permeability, magnetic induction, and the remanent magnetic induction (B_r) value also decrease with the increasing content of ferrite. This can be ascribed to the dilution effect of magnetic properties, caused by the ferrimagnetism insulation coating. All the samples with ferrite showed excellent DC properties, and the compact with 1 wt. % ferrite exhibited the best DC properties.

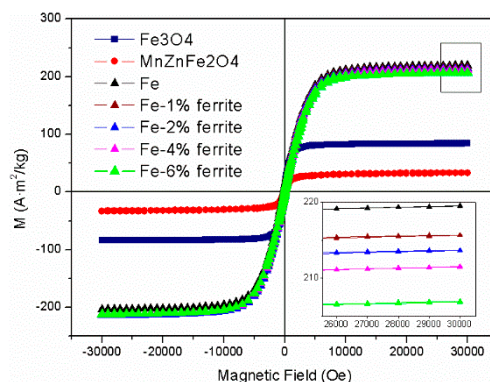


Figure 7. Magnetic hysteresis loops for Fe, $\text{Fe}/\text{Fe}_3\text{O}_4$ - $\text{MnZnFe}_2\text{O}_4$, Fe_3O_4 , and $\text{MnZnFe}_2\text{O}_4$ powders.

Table 1. Magnetic parameters for Fe, Fe/Fe₃O₄-MnZnFe₂O₄, Fe₃O₄, and MnZnFe₂O₄.

Sample	M _s (A·m ² /kg)	M _r (A·m ² /kg)	M _r /M _s
Fe	220	8.52	0.0387
Fe ₃ O ₄	84.1	8.17	0.0971
MnZnFe ₂ O ₄	33.2	5.40	0.163
Fe/1 wt. % Fe ₃ O ₄ -MnZnFe ₂ O ₄	216	0.507	0.00235
Fe/2 wt. % Fe ₃ O ₄ -MnZnFe ₂ O ₄	214	0.305	0.00143
Fe/4 wt. % Fe ₃ O ₄ -MnZnFe ₂ O ₄	212	0.122	0.000575
Fe/6 wt. % Fe ₃ O ₄ -MnZnFe ₂ O ₄	207	0.0988	0.000477

Table 2. DC performance and density for composites with different ferrite percentage.

Fe ₃ O ₄ Content (wt. %)	MnZnFe ₂ O ₄ Content (wt. %)	Density (g·cm ⁻³)	Maximum Relative Permeability	Magnetic Induction (T)	B _r (T)	H _c (Oe)
0	0	7.56	358.2	1.88	1.172	6.5
0.5	0.5	7.35	263.7	1.81	0.263	7.7
1	1	7.12	243.2	1.76	0.246	8.1
2	2	6.98	227.3	1.74	0.213	8.9
3	3	6.92	187.6	1.70	0.176	11.4

The real part and imaginary part of permeability of the Fe/Fe₃O₄-MnZnFe₂O₄ toroidal core at the frequency range of 1 kHz to 100 kHz are shown in Figure 8. The effect of Fe₃O₄-MnZnFe₂O₄ content can be clearly observed from the curves. The real part of the compacted Fe/Fe₃O₄-MnZnFe₂O₄ showed no obvious changes in the whole frequency range, while the amplitude permeability of the composite cores without ferrite decreases rapidly, which is attributed to the increase in the eddy current. The iron powder core has low electrical resistivity and resulted in a large eddy current. The eddy current increase with increasing frequency means that more reverse magnetic field is produced inside the magnet which could weaken the magnetic induction [8,20]. This conclusion is in accordance with the result of magnetic induction presented in Table 2. Moreover, the real part of permeability that exceeds 100 has been achieved, which may be due to the high density (>7.0 g/cm³) of compact, as shown in Table 2, and the relatively thin coating. With the increasing content of ferrite from 1 wt. % to 6 wt. %, the real permeability of compacts declined to nearly 90. This can be attributed to the increasing of the thickness of the Fe₃O₄-MnZnFe₂O₄ ferrite. The imaginary permeability value of the compacted Fe/Fe₃O₄-MnZnFe₂O₄ decreased from 34.5 to 14.3 when the content of ferrite decreased from 6 wt. % to 1 wt. %. The imaginary part of the compacted Fe/Fe₃O₄-MnZnFe₂O₄ exhibited a relatively low value compared with the raw Fe compact, indicating that the magnetic loss is weakened for Fe/Fe₃O₄-MnZnFe₂O₄ and can be ascribed to the high resistivity [20]. Obviously, Fe₃O₄-MnZnFe₂O₄ ferrite plays an important role in enhancing the electric resistivity of Fe powder as shown in Figure 9. With the increasing content of Fe₃O₄-MnZnFe₂O₄ ferrite in the composite, the electric resistivity increased from 98.3 mΩ·m to 733.2 mΩ·m.

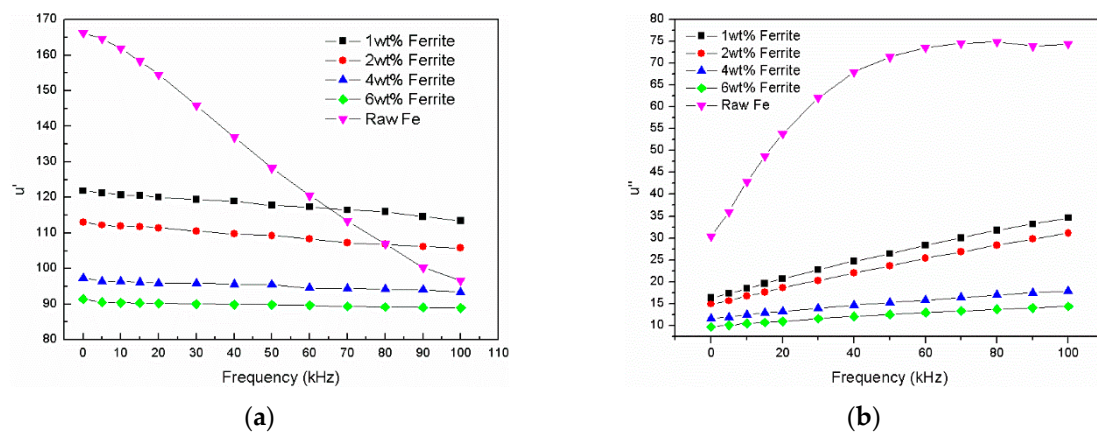


Figure 8. Permeability of Fe/Fe₃O₄-MnZnFe₂O₄ cores at frequency range of 1 kHz to 100 kHz: (a) real part permeability; (b) imaginary part permeability.

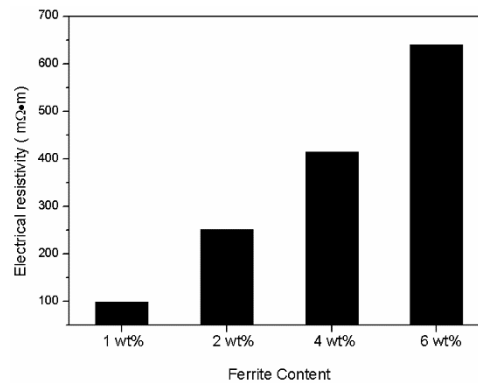


Figure 9. Resistivity of the composite compacts with different ferrite contents.

3.3. Core Loss of the Composites and Loss Separation

The total core loss of the composite with different ferrite contents dependence on frequency at 50 mT is shown in Figure 10. It can be observed that the total core loss increased significantly as the frequency increased from 5 kHz to 100 kHz. With the increasing of percentage of ferrite, the core loss decreased obviously. The composite with a 4 wt. % addition of Fe₃O₄-MnZnFe₂O₄ ferrite showed the smallest core loss compared with the raw Fe compact under the same test conditions. There exists a slight increase in the core loss of the composite with 6 wt. % ferrite (Figure 10a), which is due to the increase in hysteresis loss as shown in Figure 10b. It is well-known that the total core loss can be separated into three main parts: Hysteresis loss (P_h), eddy current loss (P_e) and residual loss (P_r). The residual loss can be ignored in the metallic materials [1]. Thus, the total core loss can be expressed by the following equation: $P_{cv} = P_h + P_e = K_h \times f + K_e \times f^2$ [1]. Where f is the frequency, K_h is the hysteresis loss coefficient and K_e is the eddy current loss coefficient.

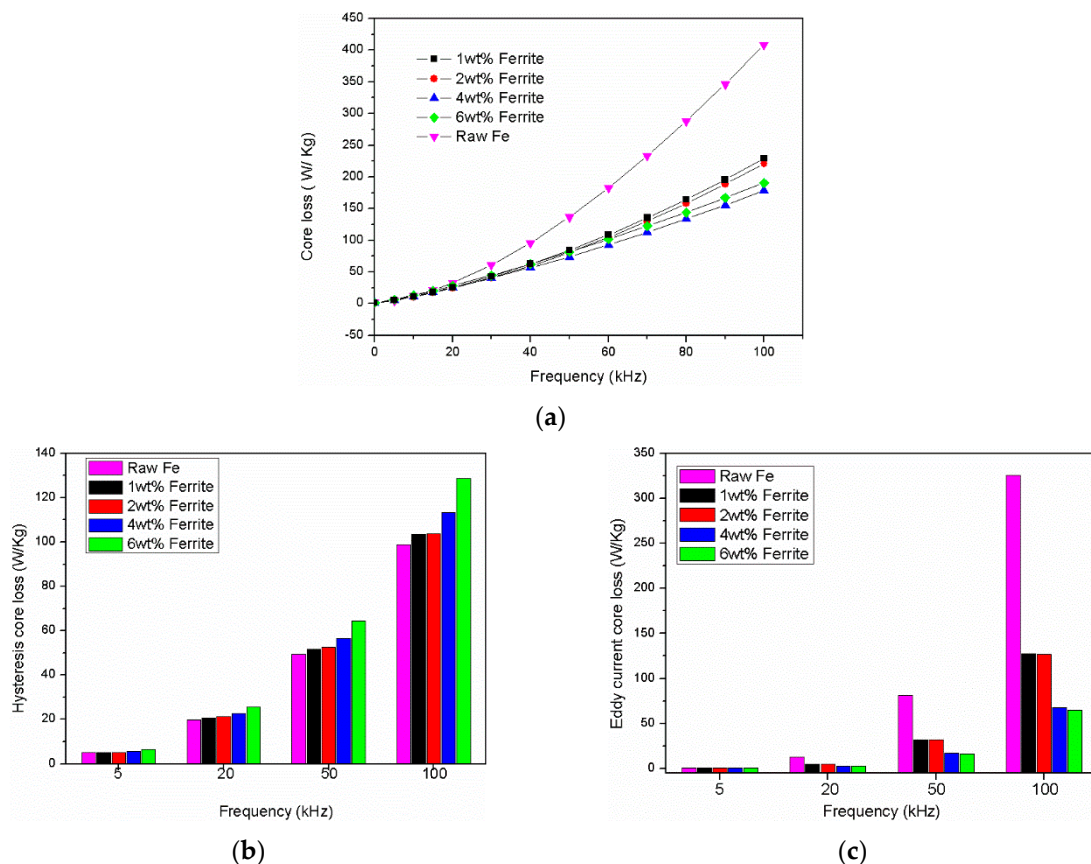


Figure 10. Core loss of the composite with different ferrite contents dependence on frequency at 0.05 T: (a) total core loss; (b) hysteresis core loss; (c) eddy current core loss.

Figure 10b,c show the value of the hysteresis loss and eddy current loss of the compacted Fe/Fe₃O₄-MnZnFe₂O₄ composite at different frequency at 50 mT with different ferrite content, which were calculated from the equation above and the obtained core loss data. As can be seen in Figure 10b, the hysteresis loss of the composite increased with the increasing content of Fe₃O₄-MnZnFe₂O₄ ferrite. Moreover, the value is larger than the hysteresis loss value of the raw Fe compact. The hysteresis loss mainly depends on the particle size, residual stress, and volume fraction of inclusions (pores, impurities, defects). The ferrite increases the distributed air gap in the composite, so that domain wall movement is difficult and increased the hysteresis loss consequently [21]. However, the eddy current loss of the Fe₃O₄-MnZnFe₂O₄ ferrite coated Fe cores was notably smaller than that of the raw Fe cores. This could be ascribed to the insulation effect caused by the Fe₃O₄-MnZnFe₂O₄ ferrite, which effectively reduced the eddy current loss.

4. Conclusions

In this work, an iron-based SMC with Fe₃O₄-MnZnFe₂O₄ insulation coating has been successfully prepared by powder metallurgy method. The co-existence of Fe₃O₄ and MnZnFe₂O₄ contributes to the preferable distribution of nano-sized insulation powders and operated as an effective insulation layer. The composite with 4wt% Fe₃O₄-MnZnFe₂O₄ ferrite exhibited excellent soft magnetic properties in general, with magnetic induction of 1.74 T, the lowest core loss, which was 178.7 W/kg (measured at 100 kHz and 50 mT) and good frequency-dependent characteristic at a wide range of frequencies. In all, the efficient preparation process and enhanced soft magnetic composite properties of the Fe/Fe₃O₄-MnZnFe₂O₄ composites promise a potential application and mass production in magnetic devices.

Author Contributions: Y.X., P.Y., and B.Y. designed the project; Y.X. performed the experiments, analyzed the data, and wrote the original draft; P.Y. and B.Y. reviewed the writing.

Funding: This research was funded by the National Key Research and Development Program of the 13th Five-Year Plan of China, grant number 2016YFB1200602-02.

Acknowledgments: I wish to thank Jianchao Xie for his help during the submission stages of this work.

Conflicts of Interest: The authors declare no conflict of interest.

References

1. Shokrollahi, H.; Janghorban, K. Soft magnetic composite materials (SMCs). *J. Mater. Process. Tech.* **2007**, *189*, 1–12. [[CrossRef](#)]
2. Guo, Y.G.; Zhu, J.G.; Zhong, J.J. Measurement and modelling of magnetic properties of soft magnetic composite material under 2D vector magnetisations. *J. Magn. Magn. Mater.* **2006**, *302*, 14–19. [[CrossRef](#)]
3. Guo, Y.G.; Zhu, J.G.; Lin, Z.W.; Zhong, J.J. 3D vector magnetic properties of soft magnetic composite material. *J. Magn. Magn. Mater.* **2006**, *302*, 511–516. [[CrossRef](#)]
4. Hamler, A.; Goričan, V.; Šuštaršič, B.; Sirc, A. The use of soft magnetic composite materials in synchronous electric motor. *J. Magn. Magn. Mater.* **2006**, *304*, 816–819. [[CrossRef](#)]
5. Gay, D.E. Soft magnetic composite materials for ac electrical applications. *Metal Powder Rep.* **1997**, *52*, 42. [[CrossRef](#)]
6. Kong, L.B.; Li, Z.W.; Liu, L.; Huang, R.; Abshinova, M.; Yang, Z.H.; Tang, C.B.; Tan, P.K.; Deng, C.R.; Matitsine, S. Recent progress in some composite materials and structures for specific electromagnetic applications. *Int. Mater. Rev.* **2013**, *58*, 203–259. [[CrossRef](#)]
7. Wang, J.; Fan, X.A.; Wu, Z.; Li, G. Intergranular insulated Fe/SiO₂ soft magnetic composite for decreased core loss. *Adv. Powder Technol.* **2016**, *27*, 1189–1194. [[CrossRef](#)]
8. Wu, S.; Sun, A.; Lu, Z.; Cheng, C.; Gao, X. Magnetic properties of iron-based soft magnetic composites with SiO₂ coating obtained by reverse microemulsion method. *J. Magn. Magn. Mater.* **2015**, *381*, 451–456. [[CrossRef](#)]
9. Wu, S.; Sun, A.; Xu, W.; Zhang, Q.; Zhai, F.; Logan, P.; Volinsky, A.A. Iron-based soft magnetic composites with Mn–Zn ferrite nanoparticles coating obtained by sol–gel method. *J. Magn. Magn. Mater.* **2012**, *324*, 3899–3905. [[CrossRef](#)]
10. Dias, M.M.; Mozetic, H.J.; Barboza, J.S.; Martins, R.M.; Pelegrini, L.; Schaeffer, L. Influence of resin type and content on electrical and magnetic properties of soft magnetic composites (SMCs). *Powder Technol.* **2013**, *237*, 213–220. [[CrossRef](#)]
11. Wu, S.; Sun, A.; Lu, Z.; Cheng, C. Fabrication and properties of iron-based soft magnetic composites coated with parylene via chemical vapor deposition polymerization. *Mater. Chem. Phys.* **2015**, *153*, 359–364. [[CrossRef](#)]
12. Kollár, P.; Birčáková, Z.; Füzér, J.; Bureš, R.; Fáberová, M. Power loss separation in Fe-based composite materials. *J. Magn. Magn. Mater.* **2013**, *327*, 146–150. [[CrossRef](#)]
13. Peng, Y.; Nie, J.; Zhang, W.; Ma, J.; Bao, C.; Cao, Y. Effect of the addition of Al₂O₃ nanoparticles on the magnetic properties of Fe soft magnetic composites. *J. Magn. Magn. Mater.* **2016**, *399*, 88–93. [[CrossRef](#)]
14. Xu, L.; Yan, B. Fe–6.5% Si/SiO₂ powder cores prepared by spark plasma sintering: Magnetic properties and sintering mechanism. *Int. J. Mod. Phys. B* **2017**, *31*, 16–19. [[CrossRef](#)]
15. Geng, K.; Xie, Y.; Xu, L.; Yan, B. Structure and magnetic properties of ZrO₂-coated Fe powders and Fe/ZrO₂ soft magnetic composites. *Adv. Powder Technol.* **2017**, *28*, 2015–2022. [[CrossRef](#)]
16. Yang, B.; Li, X.; Yang, X.; Yu, R. Chemical synthesis of Fe/Fe₃O₄ core-shell composites with enhanced soft magnetic performances. *J. Magn. Magn. Mater.* **2017**, *428*, 6–11. [[CrossRef](#)]
17. Sunday, K.J.; Hanejko, F.G.; Taheri, M.L. Magnetic and Microstructural Properties of Fe₃O₄-Coated Fe Powder Soft Magnetic Composites. *J. Magn. Magn. Mater.* **2016**, *423*, 164–170. [[CrossRef](#)]
18. Yamashita, T.; Hayes, P. Effect of curve fitting parameters on quantitative analysis of Fe_{0.94}O and Fe₂O₃ using XPS. *J. Electron Spectrosc. Relat. Phenom.* **2006**, *152*, 6–11. [[CrossRef](#)]
19. Yamashita, T.; Hayes, P. Analysis of XPS spectra of Fe²⁺ and Fe³⁺ ions in oxide materials. *Appl. Surf. Sci.* **2008**, *254*, 2441–2449. [[CrossRef](#)]

20. Li, W.; Wang, W.; Lv, J.; Ying, Y.; Yu, J.; Zheng, J.; Qiao, L.; Che, S. Structure and Magnetic Properties of Iron-based Soft Magnetic Composite with Ni-Cu-Zn Ferrite–silicone Insulation Coating. *J. Magn. Magn. Mater.* **2018**, *456*, 333–340. [[CrossRef](#)]
21. Shokrollahi, H.; Janghorban, K. Effect of warm compaction on the magnetic and electrical properties of Fe-based soft magnetic composites. *J. Magn. Magn. Mater.* **2007**, *313*, 182–186. [[CrossRef](#)]



© 2018 by the authors. Licensee MDPI, Basel, Switzerland. This article is an open access article distributed under the terms and conditions of the Creative Commons Attribution (CC BY) license (<http://creativecommons.org/licenses/by/4.0/>).